ELSEVIER

J. Non-Newtonian Fluid Mech. 122 (2004) 159–176

Journal of Non-Newtonian Fluid Mechanics

www.elsevier.com/locate/jnnfm

A new, convenient way of imposing open-flow boundary conditions in two- and three-dimensional viscoelastic flows

Xueying Xie, Matteo Pasquali*

Department of Chemical Engineering, Rice University, MS 362, 6100 Main Street, Houston, TX 77005, USA

Received 14 July 2003; received in revised form 9 February 2004; accepted 16 February 2004

This article is part of a Special Volume containing papers from the XIIIth International Workshop on Numerical Methods and Viscoelastic Flows

Abstract

Open flow boundaries are often present in viscoelastic flow calculations; their presence is not dictated by the physics of the problem, but rather by the need of truncating the computational domain. Viscoelastic liquids flowing in complex two- and three-dimensional domains are normally modeled by hyperbolic transport equations for the viscoelastic stress or conformation tensor, $\mathbf{v}\cdot\nabla\mathbf{S} = \mathcal{F}(\nabla\mathbf{v}, \mathbf{S}) - \mathcal{G}(\mathbf{S})$, where $\mathbf{S}$ is the stress or conformation tensor, $\mathbf{v}$ is the velocity, and ∇ denotes gradient in space. In steady flows, the streamlines are the characteristics of these hyperbolic equations and boundary conditions on $\mathbf{S}$ are necessary where the liquid enters the flow domain.

Open flow boundaries are almost always located in regions of fully-developed, rectilinear flow. Traditionally, several methods have been used to prescribe inflow conditions; each of them has one or more drawbacks in terms of applicability to general models, computational expense and complexity, and inability to deal with unknown flowrates, inflow-outflow boundaries, or unstructured meshes.

Here, we propose a new, general way of imposing inflow boundary conditions based on solving the coupled algebraic equations of fully developed flow at the inflow, i.e., solving the equation $\mathcal{F}(\nabla\mathbf{v}, \mathbf{S}) - \mathcal{G}(\mathbf{S}) = 0$ at the inflow coupled with the flow inside the domain. The equation holds because $\mathbf{v}\cdot\nabla\mathbf{S} \equiv 0$ in fully developed rectilinear flow. Imposing the inflow boundary condition in this fashion is fully general and does not require additional programming in solvers based on finite elements, spectral methods, and finite differences, whether or not Newton's method is used for solving the nonlinear algebraic equations arising from the discretized partial differential equation.

We test this method and find excellent agreement with analytical results in combined Poiseuille and Couette flow of Oldroyd-B and Giesekus liquids in 2-D and 3-D channels and annuli, for which analytical expressions of the velocity and conformation (elastic stress) fields are available. We demonstrate that the new method yields shorter or equal upstream lengths than traditional ones.

Keywords: Viscoelastic flow; Boundary conditions; Conformation tensor; Finite element method; Hyperbolic equations

1. Introduction

Viscoelastic flows arise in disparate processes in engineering, science, and biology—for example, in polymer processing, coating, ink-jet printing, microfluidics, geological flows in the earth mantle, hemodynamics, flow of synovial fluid in joints, and many others. Modeling viscoelastic flows is important for understanding and predicting the behavior of processes and thus for designing optimal flow configurations and for selecting operating conditions.

Open flow boundaries are often present in viscoelastic flow calculations; their presence is not dictated by the physics of the problem, but rather by the need of truncating the computational domain. For example, in polymer processing the modeling is frequently restricted to the extrusion section of the process, and the feeding section where the polymer pellets are melted is omitted from the model. Similarly, in coating processes the flow in the coating bead is the focus of the modeling, and the pumping and distribution system are often excluded from the model or they are studied separately.

Viscoelastic liquids flowing in complex two- and three-dimensional domains are generally modeled by introducing the viscoelastic stress $\boldsymbol{\sigma}$ and adding to the momentum-continuity pair an extra equation, usually of rate-type [1–7], e.g., Oldroyd-B [8,9], Giesekus [10], Leonov [11,12], PTT [13,14], FENE-P [8], FENE-CR [15], etc. More recently, viscoleastic liquids have been modeled also by in-

* Corresponding author. Tel.: +1 713 348 5830; fax: +1 713 348 5478.
E-mail address: mp@rice.edu (M. Pasquali).

0377-0257/$ – see front matter © 2004 Elsevier B.V. All rights reserved.
doi:10.1016/j.jnnfm.2004.02.011

troducing microstructural variables that represents the local state of the liquid—e.g., the conformation tensor **M** for polymer solutions [16–18]—and writing transport equations for the microstructural variables and a constitutive relationship between such microstructural variables and the viscoelastic stress [19–22]. In the absence of mass diffusion, rate-type equations for the stress and transport equations for the conformation tensor can be written as

$$\mathbf{v}\cdot\nabla\mathbf{S} = \mathcal{F}(\nabla\mathbf{v},\mathbf{S}) - \mathcal{G}(\mathbf{S}) \tag{1}$$

where **S** is the elastic stress or conformation tensor, **v** is the velocity, ∇ denotes the gradient in space, and $\mathcal{F}, \mathcal{G}$ are two tensor-valued functions (possibly nonlinear) which specify the model completely.

Eq. (1) is hyperbolic; thus, boundary conditions should be imposed at inflow boundaries to specify the state of the entering liquid. More precisely, all the components of **S** should be prescribed if a viscous stress is present in addition to the elastic stress, whereas all components but one should be prescribed when the stress is purely elastic [23]. Because open flow boundaries are introduced for computational and not physical reasons, there the distribution of elastic stress or conformation is not known in general. Thus, strategies for locating open flow boundaries and for imposing reasonable inflow boundary conditions have been an important issue in non-Newtonian fluid mechanics. The main criteria for assessing the usefulness of a boundary condition are that (1) it should yield the smallest possible computational domain, (2) it should affect only minimally the solution inside the computational domain, and (3) it should be as general as possible—i.e., it should be applicable to different models and to different computational methods.

Two chief strategies are used for locating inflow boundaries: the inflow boundary is placed in a region of weak, slowly varying flow, or the inflow boundary is placed in a region of steady, fully-developed, rectilinear flow. The first strategy yields simple boundary conditions that can be evinced from the no-flow (zeroth order in $\lambda\dot{\gamma}$), or slow-flow (first order in $\lambda\dot{\gamma}$) limiting form of Eq. (1): $\boldsymbol{\sigma} \equiv \mathbf{0}$ or $\mathbf{M} \equiv \mathbf{I}$ for no-flow, and $\boldsymbol{\sigma} \equiv 2\eta_p\mathbf{D}$ or $\mathbf{M} \equiv \mathbf{I} + 2\lambda\mathbf{D}$ for slow-flow. Here, λ is the relaxation time of the liquid, **I** is the identity tensor, $\mathbf{D} \equiv (1/2)(\nabla\mathbf{v} + \nabla\mathbf{v}^{\mathrm{T}})$ is the rate of strain, $\dot{\gamma}$ is the square root of the opposite of the second invariant (characteristic magnitude) of **D**, and η_p is the polymer (more generally, elastic) contribution to the viscosity of the liquid. Both the no-flow and the slow-flow solutions apply to generic rate-type and conformation models and can be used in various computational techniques (e.g., finite element, finite difference, and spectral methods); frequently, the slow-flow condition yields slightly smaller computational domains, although this depends on the choice of momentum boundary conditions as well.

The second strategy, i.e., placing the inflow in a steady, fully-developed, rectilinear flow region, has led to several (at least five) different implementations; each of these implementations has desirable features but none of them is free of drawbacks in terms of applicability to generic conformation-based models, computational methods (particularly in the case of finite-element methods with unstructured meshes, which is now becoming important as three-dimensional calculations are being tackled), and minimal size of the computational domain. Section 2.1 below reviews the available ways of imposing fully-developed boundary conditions on stress and conformation at inflows and highlights their pros and cons. Section 2.2 introduces a new, fully-general way of imposing the boundary condition and Section 3 details how to impose such boundary condition in the context of the finite element method. Section 4 describes the solution method. Section 5 shows that the condition works well in a number of two- and three-dimensional test cases.

2. Conformation and Stress boundary conditions for fully-developed, rectilinear flow boundaries

2.1. Standard boundary conditions

Five methods have been used in the literature to impose elastic stress or conformation boundary conditions at inflow boundaries. These methods are: (M1) using an analytical expression for $\mathbf{S}(\mathbf{x})$ [19,24–28], where **x** denotes position in the flow boundary; (M2) periodically retrieving internal values at some point far enough from the entry in the inflow region as the essential inflow boundary condition; (M3) imposing directly the condition $\mathbf{v}\cdot\nabla\mathbf{S} = \mathbf{0}$ at the inflow boundary; (M4) imposing arbitrary boundary conditions at the inflow and letting the flow develop in a long enough rectilinear region; usually, the no-flow condition is chosen for convenience ($\mathbf{M} = \mathbf{I}$ or $\boldsymbol{\sigma} = \mathbf{0}$) [29,30]; (M5) pre-computing **S** in a simple rectilinear flow geometry by imposing boundary condition (M4) on the inflow boundary and retrieving the values of **S** at the outflow, then using such retrieved values as inflow boundary conditions. Methods (M1)–(M3) come from the special form of Eq. (1) in regions of fully-developed, rectilinear flow,

$$\mathbf{v}\cdot\nabla\mathbf{S} = \mathcal{F}(\nabla\mathbf{v},\mathbf{S}) - \mathcal{G}(\mathbf{S}) \equiv \mathbf{0} \tag{2}$$

Method (M1) is based on finding once and for all an explicit analytical expression $\mathbf{S}(\nabla\mathbf{v})$ that satisfies the (usually nonlinear) equation $\mathcal{F}(\nabla\mathbf{v},\mathbf{S}) - \mathcal{G}(\mathbf{S}) \equiv \mathbf{0}$; method (M2) is based on realizing that, because $\mathbf{v}\cdot\nabla\mathbf{S} \equiv \mathbf{0}$, then $\mathbf{S}(\mathbf{x}) \equiv \mathbf{S}(\mathbf{x} + \Delta\mathbf{x})$. The other methods are self-explanatory.

A desirable method should be able to handle general equations of the form Eq. (1), should require minimal upstream length in the open flow domain for computational efficiency, should apply to structured as well as unstructured meshes, should be applicable to two-dimensional planar and axisymmetric as well as three-dimensional flows, and should be able to handle problems with unknown flowrate and with boundaries which contain both inflow and outflow portions whose location is unknown. The latter two charac-

Table 1
Methods for imposing inflow boundary conditions in regions of fully developed flow

Boundary condition	General equation	Upstream length	Unstructured mesh	3-D flows	Unknown flowrate	Backflow	Notes
Analytical (M1)	F	E	E	F	E	E	
Periodic internal boundary (M2)	E	G	D	E	E	E	1
Zero streamwise flux (M3)	E	G	F	E	E	E	2
Arbitrary (M4)	E	P	E	E	D	F	
Precomputed (M5)	E	E	D	E	F	F	3
New coupled algebraic (M6)	E	E	E	E	E	E	

Letters denote **E**xcellent, **G**ood, **P**oor, **F**ails, **D**ifficult implementation. *Notes*: (1) Method yields larger bandwidth in linear system; (2) method yields degraded accuracy near boundary; (3) enforcing the boundary condition is always cumbersome.

teristics are particularly important for the modeling of coating flows [22,31,32]. Table 1 summarizes the advantages and disadvantages of each method. Briefly, using an analytical expression—method (M1)—is always the best choice, provided that such expression is available, which is not the case for many newly-developed conformation models and also for three-dimensional flows. The periodic internal boundary method (M2) and the zero-streamwise-flux method (M3) are the next best choices, because they can handle generic conformation-tensor models; however, they do not work well on unstructured meshes and require slightly longer computational domains. The arbitrary condition method (M4) is general, but cannot handle backflow and requires long upstream sections, which is particularly undesirable in large, three-dimensional calculations. Finally, the precomputed condition method (M5) is awkward to implement and cannot handle unknown flowrate and backflow.

2.2. New method for imposing inflow boundary condition

The new boundary condition introduced here (M6) is based on imposing directly the fully developed flow equation

$$\mathcal{F}(\nabla\mathbf{v}, \mathbf{S}) - \mathcal{G}(\mathbf{S}) \equiv \mathbf{0} \tag{3}$$

as a boundary condition on the inflow section of an open boundary, and solving this equation coupled with the mass, momentum, and transport equations for stress or conformation inside the computational domain. It is a variation of method (M1) which retains all the advantageous features of the parent method and also has the important advantage that it does not require an analytical expression for stress or conformation; therefore, it is applicable to general models and to three dimensional flows (see Table 1).

The equation can be easily implemented in a node-by-node fashion in finite-difference codes, and it can be imposed readily as an essential boundary condition in low-order finite element methods as well as high-order hierarchical spectral element methods. Little effort is required for introducing this boundary condition in complex computational codes even when Newton's method with analytical Jacobian is used, because the equation and its derivatives can be obtained simply by omitting the convective terms from the full transport equations, which are already present in such codes.

3. Mathematical formulation

3.1. Field equations

In this work, the viscoelastic flow is computed by finite element method with DEVSS-TG/SUPG (Discrete Elastic-Viscous Split Stress, independent Traceless velocity Gradient interpolation, Streamline Upwind Petrov-Galerkin) which is based on successive variations on the EVSS (Elastic-Viscous Split Stress) method [2]: the elastic and viscous stress are separated explicitly (DEVSS, [33]), the entire velocity gradient is represented by continuous basis functions (DEVSS-G, [34]) and is traceless by construction (DEVSS-TG, [22]). Usually the elastic stress is represented by an independent variable which is computed by solving a rate-type constitutive equation coupled with mass and momentum conservation equation; here the conformation tensor is introduced as independent variable and the stress is related to the conformation tensor through an algebraic constitutive equation which is invoked only at the Gauss points in the finite-element solution [19,22,31].

The choice of conformation tensor is made to balance computational efficiency, thermodynamic consistency of the models, and microstructural insight. The conformation tensor is an approximate measure of the micro-structural state of a flowing viscoelastic liquid [16–18,35]. In the case of polymeric liquids, it is defined as $\mathbf{M}(\mathbf{x}, t) = \int_{\mathbf{r}\in R^3} \mathrm{d}\mathbf{r}\Psi(\mathbf{r}, \mathbf{x}, t)\mathbf{r}\mathbf{r}$, where t is time, $\mathbf{r}$ is the end-to-end connector of a polymer chain, and $\Psi(\mathbf{r}, \mathbf{x}, t)$ is the number of chains per unit mass of material whose end-to-end distance is between $\mathbf{r}$ and $\mathbf{r} + \mathrm{d}\mathbf{r}$ and whose center of mass is between $\mathbf{x}$ and $\mathbf{x} + \mathrm{d}\mathbf{x}$ at time t. The eigenvectors of $\mathbf{M}$ represent the principal directions along which the polymer chains are stretched, contracted, or oriented. The eigenvalues of the dimensionless conformation tensor $\mathbf{M}$ represent the square of the principal stretch ratios. Computational models based on conformation tensor are no more expensive than models based on rate-type equations for the viscoelastic stress, yet much cheaper than models based on more detailed microstructural representations of the liquid based on bead-spring-rod models—e.g., stochastic methods such as CONFFESSIT [36], Adaptive Lagrangian Particle [37], and Brownian Configuration Fields [38], as well as Fokker–Planck methods [39]. However, compared to rate-type equations, conformation tensor models allow a much

Table 2
Computational error on the components of velocity and conformation computed on a 16×16 mesh at $We = 1 \sim 9.28$, $\beta = 0.59$ in the 2-D channel

Weissenberg number	Velocity and conformation	Maximum numerical value	Maximum absolute error	Relative error (%)
$We = 1$	v_x	1.10×10^{-1}	7.79×10^{-5}	0.07
	v_y	9.27×10^{-6}	9.27×10^{-6}	N/A
	M_{yy}	1.00	2.00×10^{-4}	0.02
	M_{xy}	1.00	5.45×10^{-4}	0.05
	M_{xx}	3.00	5.85×10^{-3}	0.20
$We = 3.77$	v_x	1.10×10^{-1}	1.76×10^{-4}	0.16
	v_y	4.84×10^{-5}	4.84×10^{-5}	N/A
	M_{yy}	1.00	5.70×10^{-3}	0.57
	M_{xy}	3.78	2.63×10^{-2}	0.70
	M_{xx}	29.51	1.50×10^{-1}	0.51
$We = 5$	v_x	1.10×10^{-1}	3.73×10^{-4}	0.34
	v_y	1.22×10^{-4}	1.22×10^{-4}	N/A
	M_{yy}	1.02	2.23×10^{-2}	2.23
	M_{xy}	5.05	1.61×10^{-1}	3.21
	M_{xx}	51.65	1.28	2.50
$We = 9.28$	v_x	1.11×10^{-1}	3.06×10^{-3}	2.78
	v_y	1.17×10^{-4}	1.17×10^{-4}	N/A
	M_{yy}	1.13	1.30×10^{-1}	13.0
	M_{xy}	9.31	7.94×10^{-1}	8.55
	M_{xx}	171.27	$1.12 \times 10^{+1}$	6.48

The new conformation boundary condition (M6) is imposed at the inflow regions. The relative error is calculated by dividing the maximum absolute error by the corresponding maximum value obtained with the analytical solution.

Table 3
Computational error on the components of velocity and conformation computed on a 16×16 mesh at $We = 3$ and 3.77, $\beta = 0.59$ in the 2-D channel

Weissenberg number	Velocity and conformation	Maximum numerical value	Maximum absolute error	Relative error (%)
$We = 3$	v_x	1.10×10^{-1}	7.34×10^{-5}	0.09
	v_y	9.53×10^{-9}	9.53×10^{-9}	N/A
	M_{yy}	1.00	0	0
	M_{xy}	3.00	1.08×10^{-3}	0.04
	M_{xx}	18.95	4.12×10^{-2}	0.22
$We = 3.77$	v_x	1.11×10^{-1}	1.83×10^{-3}	1.66
	v_y	3.18×10^{-4}	3.18×10^{-4}	N/A
	M_{yy}	1.16	1.60×10^{-1}	16.0
	M_{xy}	4.92	1.35	35.89
	M_{xx}	43.60	$1.42 \times 10^{+1}$	48.16

No boundary condition is imposed on the conformation tensor. The relative error is calculated by dividing the maximum absolute error by the corresponding maximum value obtained with the analytical solution.

Table 4
Computational error on the components of conformation computed on a sequence of increasingly refined meshes with the Oldroyd-B model at $We = 3.0$, $\beta = 0.59$ in the 2-D channel

Mesh size	Conformation	Maximum numerical value	Maximum absolute error	Relative error (%)
8×8	M_{yy}	1.00	2.00×10^{-3}	0.20
	M_{xy}	3.00	1.07×10^{-2}	0.36
	M_{xx}	18.86	2.38×10^{-1}	1.25
12×12	M_{yy}	1.00	1.53×10^{-3}	0.15
	M_{xy}	3.00	5.60×10^{-3}	0.19
	M_{xx}	18.92	1.08×10^{-1}	0.57
16×16	M_{yy}	1.00	9.60×10^{-4}	0.10
	M_{xy}	3.00	4.45×10^{-3}	0.15
	M_{xx}	18.94	6.40×10^{-2}	0.34
20×20	M_{yy}	1.00	9.10×10^{-4}	0.09
	M_{xy}	3.00	3.90×10^{-3}	0.13
	M_{xx}	19.01	4.20×10^{-2}	0.22

The relative error is calculated by dividing the maximum absolute error by the corresponding maximum value obtained with the analytical solution.

Table 5
Computational error on the components of the conformation tensor in axisymmetric pipe flow of an Oldroyd-B liquid at $We = 1$ to 4, $\beta = 0.59$; computed as three-dimensional flow on an unstructured tetrahedral mesh with average size $0.25R$

We	Conformation	Maximum numerical value	Maximum absolute error	Relative error (%)
$We = 1$	M_{11}	3.01	7.66×10^{-2}	2.55
	M_{12}	1.00	7.58×10^{-3}	0.76
	M_{13}	1.00	5.95×10^{-3}	0.60
	M_{22}	1.00	3.17×10^{-3}	0.32
	M_{23}	1.70×10^{-3}	1.70×10^{-3}	N/A
	M_{33}	1.00	2.60×10^{-3}	0.26
$We = 2$	M_{11}	9.01	4.31×10^{-1}	4.79
	M_{12}	1.99	3.64×10^{-2}	1.82
	M_{13}	2.01	3.64×10^{-2}	1.82
	M_{22}	1.01	1.36×10^{-2}	1.36
	M_{23}	7.18×10^{-3}	7.18×10^{-3}	N/A
	M_{33}	1.01	1.24×10^{-2}	1.24
$We = 4$	M_{11}	35.11	3.98	12.06
	M_{12}	4.40	4.90×10^{-1}	12.3
	M_{13}	4.11	7.12×10^{-1}	17.8
	M_{22}	1.11	1.08×10^{-1}	10.8
	M_{23}	7.73×10^{-2}	7.73×10^{-2}	N/A
	M_{33}	1.08	1.15×10^{-1}	11.5

The relative error is calculated by dividing the maximum absolute error in each component by the corresponding maximum analytical value of that component.

richer description of the liquid microstructure and also ensure that the the thermodynamic-based relationship between microstructure and viscoelastic stress is always respected [16–18,31,35].

The coupled transport equations of mass, momentum and conformation, together with the velocity gradient interpolation equation in steady, incompressible viscoelastic flow are

$$0 = \nabla \cdot \mathbf{v} \tag{4}$$

$$\mathbf{0} = \rho \mathbf{v} \cdot \nabla \mathbf{v} - \nabla \cdot \mathbf{T} - \rho \mathbf{g} \tag{5}$$

$$\mathbf{0} = \mathbf{L} - \nabla \mathbf{v} + \frac{1}{\mathrm{tr}\,\mathbf{I}} (\nabla \cdot \mathbf{v}) \mathbf{I} \tag{6}$$

$$\begin{aligned} \mathbf{0} = & -\mathbf{v} \cdot \nabla \mathbf{M} + 2\xi \frac{\mathbf{D} : \mathbf{M}}{\mathbf{I} : \mathbf{M}} \mathbf{M} \\ & + \zeta \left(\mathbf{M} \cdot \mathbf{D} + \mathbf{D} \cdot \mathbf{M} - 2 \frac{\mathbf{D} : \mathbf{M}}{\mathbf{I} : \mathbf{M}} \mathbf{M} \right) + \mathbf{M} \cdot \mathbf{W} \\ & + \mathbf{W}^{\mathrm{T}} \cdot \mathbf{M} - \frac{1}{\lambda} (g_0 \mathbf{I} + g_1 \mathbf{M} + g_2 \mathbf{M}^2) \end{aligned} \tag{7}$$

where ρ is the material density, $\mathbf{g}$ is the body force per unit mass, $\mathbf{T}$ is the stress tensor, $\mathbf{L}$ is the interpolated velocity gradient, $\xi(\mathbf{M})$ and $\zeta(\mathbf{M})$ are the polymer resistance to stretching and orientation, $\mathbf{D} \equiv \frac{1}{2}(\mathbf{L} + \mathbf{L}^{\mathrm{T}})$ is the rate of strain, $\mathbf{W} \equiv \frac{1}{2}(\mathbf{L} - \mathbf{L}^{\mathrm{T}})$ is the vorticity, λ is the characteristic relaxation time, and $g_0(\mathbf{M})$, $g_1(\mathbf{M})$ and $g_2(\mathbf{M})$ are relaxation functions. $\mathbf{T}$ is the total (Cauchy) stress; it can be split into 3 parts,

$$\mathbf{T} = -p\mathbf{I} + \boldsymbol{\tau} + \boldsymbol{\sigma} \tag{8}$$

where p is the pressure, $\boldsymbol{\tau}$ is the viscous stress which in DEVSS is related to the raw and interpolated velocity gradients as [22,31]

$$\boldsymbol{\tau} = \eta_{\mathrm{s}} (\mathbf{L} + \mathbf{L}^{\mathrm{T}}) + \eta_{\mathrm{a}} (\nabla \mathbf{v} + \nabla \mathbf{v}^{\mathrm{T}} - \mathbf{L} - \mathbf{L}^{\mathrm{T}}) \tag{9}$$

where η_{s} is solvent viscosity, η_{a} is a numerical parameter that stabilizes the computational method [33] and should be comparable to the total viscosity $\mu \equiv \eta_{\mathrm{s}} + \eta_{\mathrm{p}}$ of the liquid.

The elastic stress $\boldsymbol{\sigma}$ is related to the conformation tensor through an equation of state [16,31,35,40]

$$\begin{aligned} \underbrace{\boldsymbol{\sigma}}_{\text{elastic stress}} = & \underbrace{2\xi \frac{\mathbf{M}}{\mathbf{I} : \mathbf{M}} \mathbf{M} : \frac{\partial a}{\partial \mathbf{M}}}_{\text{stress by molecular stretching}} \\ & + \underbrace{2\zeta \left(-\frac{\mathbf{M}}{\mathbf{I} : \mathbf{M}} \mathbf{M} : \frac{\partial a}{\partial \mathbf{M}} + \mathbf{M} \cdot \frac{\partial a}{\partial \mathbf{M}} \right)}_{\text{stress by molecular orientation}} \end{aligned} \tag{10}$$

where $a(\mathbf{M})$ is the Helmholtz free energy per unit volume of the polymeric liquid; the specific form of this function depends on the choice of conformation tensor model.

3.2. Momentum boundary conditions

Boundary conditions on the momentum equation must be specified on all boundaries. The conformation tensor equation is hyperbolic; thus, boundary conditions are required only at inflow boundaries, i.e., where $\mathbf{n} \cdot \mathbf{v} < 0$. The boundary conditions for conformation tensor equations have been detailed in Section 2; those on the momentum equation are listed here.

Table 6
Computational error on the components of the conformation tensor in axisymmetric pipe flow of an Oldroyd-B liquid at $We = 1$, $\beta = 0.59$; computed as three-dimensional flow on seven increasingly refined unstructured tetrahedral meshes

Mesh	Conformation	Maximum numerical value	Maximum absolute error	Relative error (%)
$h = 0.12R$, elements = 27293, nodes = 39482	M_{11}	3.00	1.98×10^{-2}	0.66
	M_{12}	1.00	2.16×10^{-3}	0.22
	M_{13}	1.00	2.13×10^{-3}	0.21
	M_{22}	1.00	8.30×10^{-4}	0.08
	M_{23}	4.84×10^{-4}	4.84×10^{-4}	N/A
	M_{33}	1.00	9.10×10^{-4}	0.09
$h = 0.14R$, elements = 16092, nodes = 23824	M_{11}	3.00	3.02×10^{-2}	1.01
	M_{12}	1.00	2.19×10^{-3}	0.22
	M_{13}	1.00	2.28×10^{-3}	0.23
	M_{22}	1.00	1.12×10^{-3}	0.11
	M_{23}	6.94×10^{-4}	6.94×10^{-4}	N/A
	M_{33}	1.00	1.20×10^{-3}	0.12
$h = 0.20R$, elements = 5666, nodes = 8702	M_{11}	3.00	5.36×10^{-2}	1.76
	M_{12}	1.00	4.76×10^{-3}	0.48
	M_{13}	1.00	4.41×10^{-3}	0.44
	M_{22}	1.00	1.85×10^{-3}	0.19
	M_{23}	9.65×10^{-4}	9.65×10^{-4}	N/A
	M_{33}	1.00	2.00×10^{-3}	0.20
$h = 0.25R$, elements = 2911, nodes = 4654	M_{11}	3.01	7.66×10^{-2}	2.55
	M_{12}	1.00	7.58×10^{-3}	0.76
	M_{13}	1.00	5.95×10^{-3}	0.60
	M_{22}	1.00	3.17×10^{-3}	0.32
	M_{23}	1.70×10^{-3}	1.70×10^{-3}	N/A
	M_{33}	1.00	2.60×10^{-3}	0.26
$h = 0.30R$, elements = 1796, nodes = 2928	M_{11}	3.01	9.09×10^{-2}	3.03
	M_{12}	1.00	6.95×10^{-3}	0.70
	M_{13}	1.00	6.90×10^{-3}	0.70
	M_{22}	1.00	2.90×10^{-3}	0.29
	M_{23}	1.57×10^{-3}	1.57×10^{-3}	N/A
	M_{33}	1.00	2.70×10^{-3}	0.27
$h = 0.35R$, elements = 1125, nodes = 1892	M_{11}	3.00	1.34×10^{-1}	4.47
	M_{12}	1.00	6.72×10^{-3}	0.67
	M_{13}	1.00	8.43×10^{-3}	0.84
	M_{22}	1.00	2.79×10^{-3}	0.28
	M_{23}	1.81×10^{-3}	1.81×10^{-3}	N/A
	M_{33}	1.00	4.30×10^{-3}	0.43
$h = 0.45R$, elements = 547, nodes = 989	M_{11}	3.02	1.87×10^{-1}	6.22
	M_{12}	1.00	1.72×10^{-2}	1.72
	M_{13}	1.00	1.22×10^{-2}	1.22
	M_{22}	1.01	5.10×10^{-3}	0.51
	M_{23}	2.63×10^{-3}	2.63×10^{-3}	N/A
	M_{33}	1.01	5.90×10^{-3}	0.59

The relative error is calculated by dividing the maximum absolute error in each component by the corresponding maximum analytical value of that component.

(1) No slip and no penetration: at solid, impermeable boundaries, the velocity of the liquid equals that of solid, i.e. $\mathbf{v} = \mathbf{v}_w$, where $\mathbf{v}_w$ is the solid wall velocity; this condition is applied by replacing the momentum residual (i.e., essentially).
(2) Inflow and outflow conditions; one of the following three conditions can be imposed: (i) imposed velocity profile $\mathbf{v} = \mathbf{v}_0$ (imposed essentially); (ii) imposed pressure $p = p_0$ (imposed through the boundary integral of the traction in the momentum equation, i.e., naturally); (iii) imposed fully developed flow, i.e. $\mathbf{n} \cdot \nabla\mathbf{v} = 0$ (imposed naturally), possibly in conjunction with the imposed pressure condition (see [41,42]). The latter two boundary conditions are imposed through the weighted residual integral of the traction $\mathbf{n} \cdot \mathbf{T}$ at a boundary Γ as follows:

$$\int_\Gamma \psi^\beta \underbrace{\mathbf{n} \cdot \mathbf{T}}_{\text{traction}} \, \mathrm{d}\Gamma = \int_\Gamma \psi^\beta (\underbrace{-\hat{p}\mathbf{n}}_{\text{traction from pressure}} + \underbrace{\mathbf{n} \cdot \boldsymbol{\sigma}}_{\text{traction from elastic stress}} + \underbrace{\mathbf{n} \cdot (\eta_s \mathbf{L}^{\mathrm{T}} + \eta_a(\nabla\mathbf{v}^{\mathrm{T}} - \mathbf{L}^{\mathrm{T}}))}_{\text{traction from viscous stress}} + \underbrace{f\mathbf{n} \cdot (\eta_s \mathbf{L} + \eta_a(\nabla\mathbf{v} - \mathbf{L}))}_{\text{traction from viscous stress}}) \, \mathrm{d}\Gamma \tag{11}$$

Table 7
Computational error on the components of the conformation tensor in axisymmetric annular flow of an Oldroyd-B liquid at $We = 0.7$ to 2, $\beta = 0.59$; computed as three-dimensional flow on an unstructured tetrahedral mesh (Fig. 11, right)

We	Conformation	Maximum numerical value	Maximum absolute error	Relative error (%)
$We = 0.7$	M_{11}	2.00	9.96×10^{-2}	5.05
	M_{12}	0.70	1.18×10^{-2}	1.69
	M_{13}	0.70	1.38×10^{-2}	1.98
	M_{22}	1.00	2.91×10^{-3}	0.29
	M_{23}	2.00×10^{-3}	2.00×10^{-3}	N/A
	M_{33}	1.00	3.48×10^{-3}	0.35
$We = 1$	M_{11}	3.08	2.02×10^{-1}	6.75
	M_{12}	1.00	1.73×10^{-2}	1.73
	M_{13}	1.00	2.13×10^{-2}	2.13
	M_{22}	1.00	5.90×10^{-3}	0.59
	M_{23}	4.01×10^{-3}	4.01×10^{-3}	N/A
	M_{33}	1.00	6.61×10^{-3}	0.66
$We = 2$	M_{11}	10.46	1.46	16.20
	M_{12}	2.03	1.27×10^{-1}	6.35
	M_{13}	2.07	1.08×10^{-1}	5.39
	M_{22}	1.02	2.29×10^{-2}	2.29
	M_{23}	2.56×10^{-2}	2.56×10^{-2}	N/A
	M_{33}	1.03	3.04×10^{-2}	3.04

The relative error is calculated by dividing the maximum absolute error in each component by the corresponding maximum analytical value of that component.

where ψ^β are the weighting functions of the momentum equation. If the pressure p_0 is known at the boundary Γ, then $\hat{p} \equiv p_0$, otherwise the pressure is computed from the finite element basis functions and coefficients, i.e., $\hat{p} \equiv p^\alpha \phi^\alpha$ (sum on α); if $\mathbf{n} \cdot \nabla \mathbf{v} = 0$, then the coefficient f is set to $f \equiv 0$, otherwise f is set to $f \equiv 1$. The remaining quantities in equation 11 are computed by using the finite element basis functions and coefficients. This boundary condition is related to the "no boundary condition" of Papanastasiou et al. [43–45], which is recovered by setting both $f \equiv 1$ and $\hat{p} \equiv p^\alpha \phi^\alpha$.

(3) Symmetry: at a symmetry line or plane, the normal component of the velocity and the tangential components of the traction vanish; thus, $\mathbf{n} \cdot \mathbf{v} = 0$ and $\mathbf{t}_i \mathbf{n} : \mathbf{T} = 0$ ($i = 1, 2$ in three-dimensional flows). The boundary condition $\mathbf{n} \cdot \mathbf{v} = 0$ is imposed essentially at the boundary nodes (i.e., by replacing the normal component of the momentum equation). The boundary conditions $\mathbf{t}_i \mathbf{n} : \mathbf{T} = 0$ are imposed naturally (i.e., by setting to zero the tangential components of the traction in the boundary integral of the momentum equation weighted residual).

3.3. New conformation boundary condition

The transport equation of conformation (Eq. (7)) can be recast in the form of Eq. (1) by setting

$$\mathcal{F}(\nabla \mathbf{v}, \mathbf{M}) \equiv 2(\xi - \zeta)\frac{\mathbf{D} : \mathbf{M}}{\mathbf{I} : \mathbf{M}}\mathbf{M} + \zeta(\mathbf{M} \cdot \mathbf{D} + \mathbf{D} \cdot \mathbf{M}) + \mathbf{M} \cdot \mathbf{W} + \mathbf{W}^{\mathrm{T}} \cdot \mathbf{M} \quad (12)$$

$$\mathcal{G}(\mathbf{M}) \equiv \frac{1}{\lambda}(g_0 \mathbf{I} + g_1 \mathbf{M} + g_2 \mathbf{M}^2) \quad (13)$$

which yields the form of the new boundary condition for conformation tensor models

$$0 = -2\xi\frac{\mathbf{D} : \mathbf{M}}{\mathbf{I} : \mathbf{M}}\mathbf{M} - \zeta\left(\mathbf{M} \cdot \mathbf{D} + \mathbf{D} \cdot \mathbf{M} - 2\frac{\mathbf{D} : \mathbf{M}}{\mathbf{I} : \mathbf{M}}\mathbf{M}\right) - \mathbf{M} \cdot \mathbf{W} - \mathbf{W}^{\mathrm{T}} \cdot \mathbf{M} + \frac{1}{\lambda}(g_0 \mathbf{I} + g_1 \mathbf{M} + g_2 \mathbf{M}^2) \quad (14)$$

Eq. (14) is a nonlinear algebraic equation in the variables $\mathbf{D}, \mathbf{W}$, and $\mathbf{M}$. It is imposed essentially by replacing the finite element residuals associated with the relevant non-vanishing conformation basis functions at the inflow boundary nodes (where $\mathbf{n} \cdot \mathbf{v} < 0$) with the residuals of Eq. (14) at the boundary nodes, and solved coupled with the flow equations; whether each boundary node is an inflow of an outflow node is determined at each Newton iteration by taking the scalar product of the current approximation of the velocity field with the normal to the boundary ([31] for details). Because the same constitutive functions ξ, ζ, g_0, g_1, g_2, and a appear in the transport equation of conformation, in the constitutive equation of the viscoelastic stress, and in the inflow boundary conditions, the computational code does not need to be changed when switching from a constitutive model to another. Thus, the new boundary condition conveniently overcomes the disadvantages of method (M1).

Of course, if the problem equations are cast and solved in the stress-velocity-pressure formulation instead of the conformation-velocity-pressure formulation, the algebraic part of the constitutive equation is im-

posed as essential boundary condition at the inflow nodes.

3.4. Specific conformation-tensor models

Three different conformation tensor models are used below: Oldroyd-B [8,9], Giesekus [10], and FENE-P [8].

The constitutive functions of the Oldroyd-B model are $\xi = 1$, $\zeta = 1$, $g_0 = -1$, $g_1 = 1$, $g_2 = 0$, and $\partial a/\partial \mathbf{M} = (G/2)\mathbf{I}$, where $G \equiv \eta_p/\lambda$ is the polymer modulus.

The constitutive functions of the Giesekus model are identical to those of the Oldroyd-B, except for the relaxation terms $g_0 = \alpha - 1$, $g_1 = 1 - 2\alpha$, $g_2 = \alpha$, where α is a dimensionless parameter that describes the degree of anisotropic drag in the liquid and controls the shear thinning (the Oldroyd-B is recovered by setting $\alpha = 0$).

The FENE-P model has the same constitutive functions of the Oldroyd-B except for the function $g_1 = (b-1)/(b - I_M/3)$, which describes the fast relaxation of highly extended polymer chains, and the expression of the free energy $\partial a/\partial \mathbf{M} = (G/2)(b-1)/(b - I_{\mathbf{M}}/3)\mathbf{I}$; here $I_{\mathbf{M}} \equiv \mathbf{I} : \mathbf{M}$ is the first invariant (trace) of $\mathbf{M}$. The dimensionless parameter b represents the molecular extensibility, and it equals to the square of the ratio between the contour length of polymer chains and their equilibrium end-to-end distance.

3.5. Dimensionless numbers

In addition to the model-specific parameters α and b, it is convenient to introduce three dimensionless numbers. The Reynolds number $Re \equiv \rho v d/\mu$ characterizes the balance between inertial and surface (viscous and viscoelastic) forces, where v and d are the characteristic velocity and length of a flow; hereafter $Re \equiv 0$.

The solvent viscosity ratio $\beta \equiv \eta_s/(\eta_s + \eta_p) \equiv \eta_s/\mu$ characterizes the relative importance of viscous and viscoelastic stresses.

The Weissenberg number $We \equiv \lambda \dot{\gamma}_c$ represents the intensity of the flow on the timescale of the relaxation time of the polymer conformation. $\dot{\gamma}_c$ is a characteristic shear rate, which is defined below for each flow studied here.

4. Solution method

The DEVSS-TG/SUPG Finite Element Method is applied to reduce the partial differential equations of the flow to algebraic equations. The details are presented elsewhere [22,31]; because the method and computational code represents variables and residual equations as vectors and tensors [22], the extension to three-dimensions is straightforward if free surfaces and deformable boundaries are absent. Structured quadrilateral elements are used in two-dimensional problems. Velocity basis functions are biquadratic and continuous, velocity gradient, conformation basis functions are bilinear and continuous, and pressure basis functions are linear and discontinuous. In 3-D problems, unstructured tetrahedral elements are used. The basis functions for velocity are quadratic and continuous, those for pressure, velocity gradient and conformation are linear and continuous. The fully coupled set of nonlinear algebraic equations is solved by Newton's method with analytical Jacobian, which yields a large scale linear algebraic system $\boldsymbol{J}\Delta\boldsymbol{x} = -\boldsymbol{r}$, where $\boldsymbol{J}$ is the Jacobian matrix, $\Delta\boldsymbol{x}$ is the Newton update, and $\boldsymbol{r}$ is the residual vector. A direct frontal solver [46] parallelized by OpenMP is employed to solve the linear system in two-dimensional flows. Because in three dimensions the number of algebraic equations is larger and because a direct method would generate excessive fill-in in the LU factors of the Jacobian matrix, restarted GMRES [47,48] is used to solve the linear system. Because the Jacobian matrix $\boldsymbol{J}$ has zero diagonal entries associated with incompressibility and also small diagonal entries associated with the viscoelastic momentum balance at high Weissenberg number, an Incomplete LU preconditioner is applied to speed the convergence rate of GMRES. The results presented here were computed on an IBM Regatta with 64 GB shared memory and 16 Power4 processors running at 1.33 GHz .

5. Testing the new boundary condition

The proposed new boundary condition is tested in both two- and three-dimensional flows where exact analytical solutions are known for certain conformation-based models. These flows are: (1) a combination of drag (Couette) and pressure-driven (Poiseuille) flow in a planar two-dimensional channel; (2) pressure-driven flow in a three-dimensional pipe; and (3) a combination of drag and pressure-driven flow in a three-dimensional annulus. The pipe and the annulus are chosen as axisymmetric in order to obtain analytical solutions to the flow problem, but they are treated as three-dimensional domains in the computational problem. The new boundary is also compared with traditional boundary conditions in a two-dimensional flow around a cylinder.

5.1. Two-dimensional flow in a planar channel

Fig. 1 shows a combination of Poiseuille and Couette flow in a planar channel of height b and length $L \equiv 4b$, together with the boundary conditions. The combination of Poiseuille flow (which is pushing liquid from left to right) and Couette flow (which is dragging liquid from right to left), generates two inflow sections, one on each open flow boundary. The new boundary condition is imposed on these two inflow sections. The Oldroyd-B and Giesekus models are tested in this flow because analytical solutions are available for validating the numerical results.

A pressure difference $p_1 - p_2$ is imposed between the two open flow boundaries through the traction term in the momentum residual; the top boundary is stationary and the bottom one is moving with velocity u_0 in the direction of decreasing x. v_x and v_y are velocities in x and y

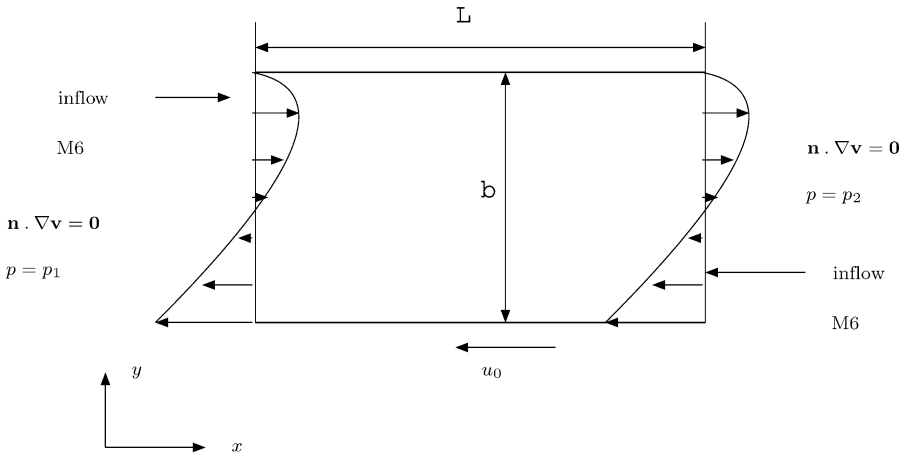

Fig. 1. Geometry and boundary conditions for the two-dimensional planar channel flow. The pressure difference drives flow from left to right, the moving bottom wall drags flow from right to left; thus, both open-flow boundaries have inflow and outflow sections.

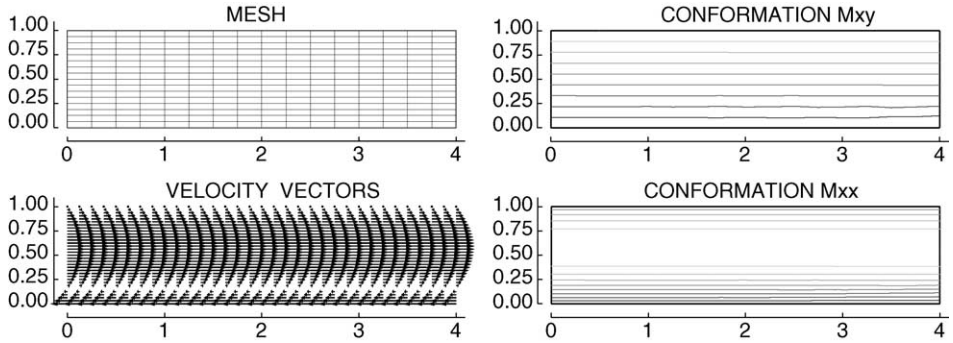

Fig. 2. Left: 16×16 mesh used for computing the flow in the two-dimensional planar channel, computed velocity vectors (showing that both boundaries have inflow as well as outflow sections). Right: contour lines of the non-trivial conformation components ($M_{yy} \equiv 1$ here). Computed with the Oldroyd-B model at $We = 5$, $\beta = 0.59$.

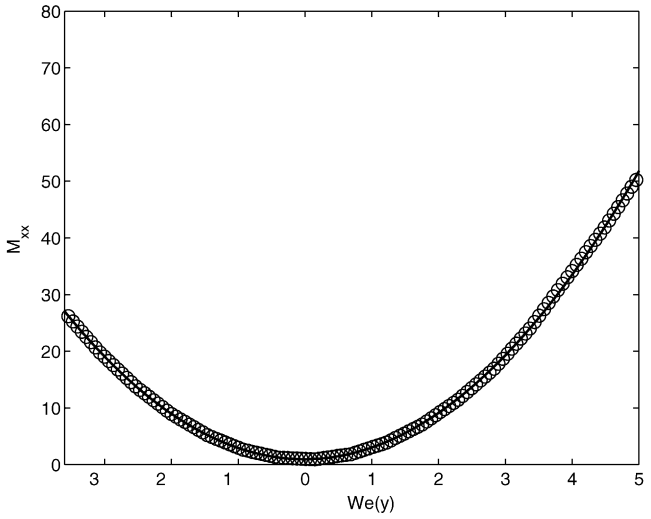

Fig. 3. Streamwise conformation component M_{xx} vs. local dimensionless shear rate $We(y) \equiv \lambda L_{yx}$ at the right ($x \equiv L$) section of the flow in a planar channel, computed on the 16×16 mesh with the Oldroyd-B at $We = 5$, $\beta = 0.59$. The open circles denote the computed values, the solid line is the analytical solution $M_{xx} = 1 + 2We^2(y)$.

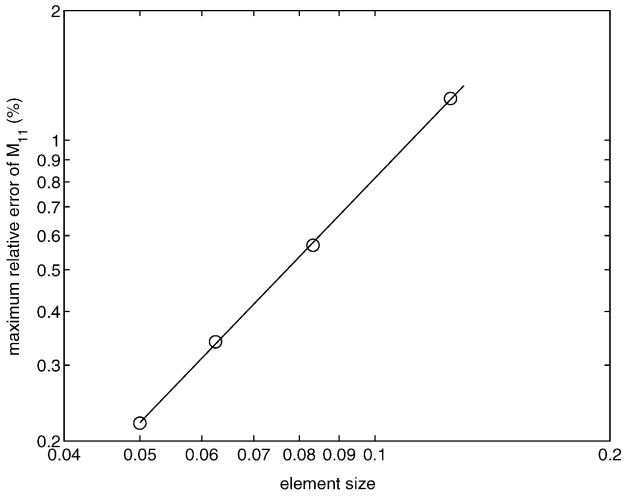

Fig. 4. Convergence rate of the solution computed in the flow in the planar channel with the Oldroyd-B model at $\beta = 0.59$, $We = 3$. The symbols denote the maximum relative error e on the conformation component M_{11} versus the dimensionless element size h. The solid line is the best fit $\log(e) = 1.89 \log(h) + 1.80$.

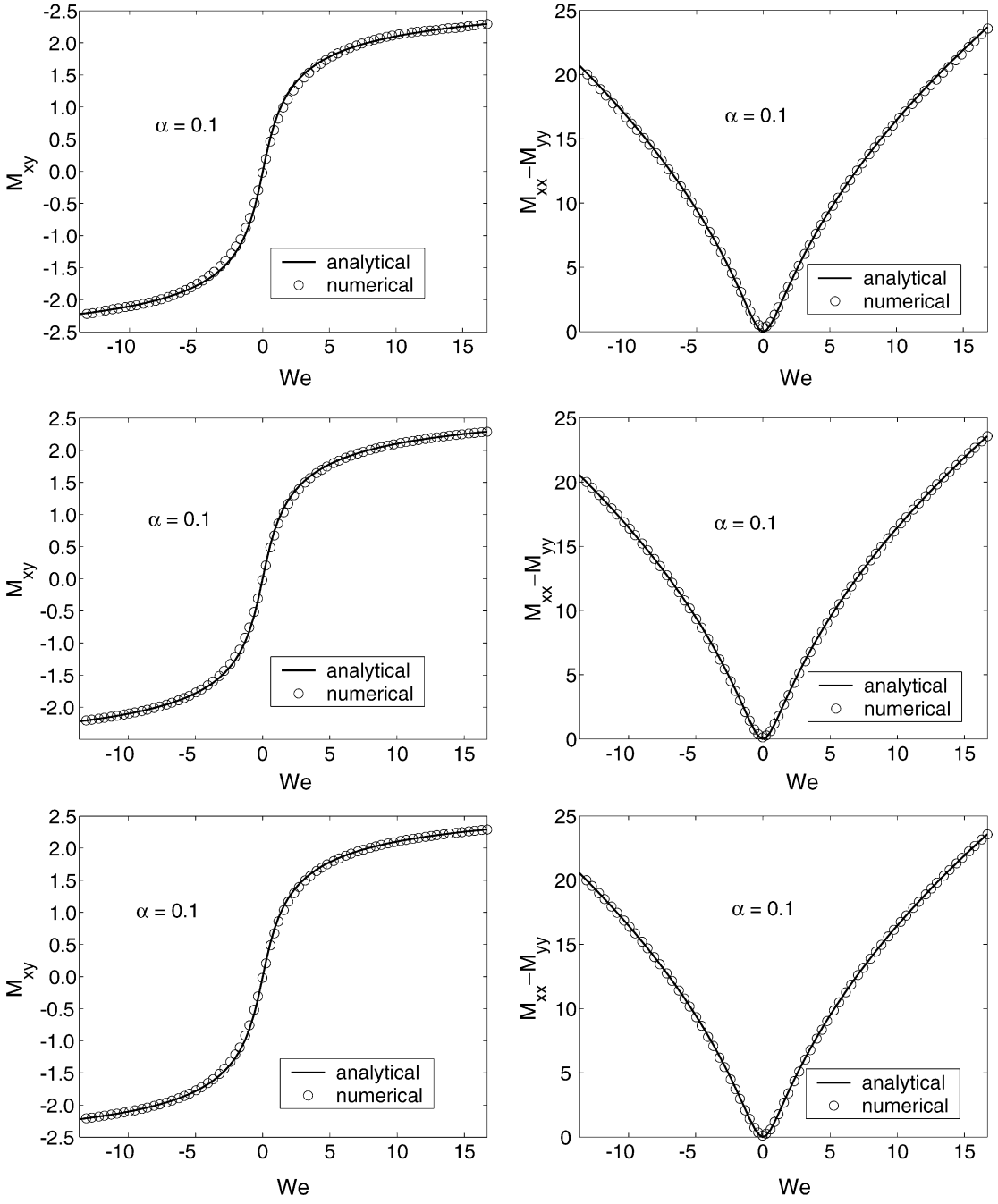

Fig. 5. Off-diagonal component of the conformation tensor M_{xy} (left) and difference between the diagonal (normal) components of the conformation tensor $M_{xx} - M_{yy}$ (right) vs. local dimensionless shear rate $We(y) \equiv \lambda L_{yx}$ computed in the planar channel flow with the Giesekus model ($\beta = 0.59$, $\alpha = 0.1$). The profiles are reported at the $x = 0$ boundary (top), $x = L/2$ channel section (middle), and $x = L$ boundary (bottom). The symbols denote the computational results, the solid lines are the analytical solutions Eq. (21) and Eq. (22).

directions respectively. The computation is carried out at $\Delta p \equiv (p_1 - p_2)b/(\mu u_0) = 50$, $\beta = 0.59$. The characteristic Weissenberg number of the flow is $We \equiv \lambda\dot{\gamma}_c$, where $\dot{\gamma}_c \equiv (\Delta pb/(2L) + 1)(u_0/b)$ is the maximum shear rate based on the Newtonian (constant μ) velocity profile; the Weissenberg number is initially set to $We = 1$ and is then increased by continuation.

The analytical expressions of velocity, velocity gradient, and conformation are

$$v_x = \left[-\frac{\Delta p}{2}\frac{b}{L}\left(\left(\frac{y}{b}\right)^2 - \frac{y}{b}\right) + \frac{y}{b} - 1\right]u_0 \tag{15}$$

$$v_y = 0 \tag{16}$$

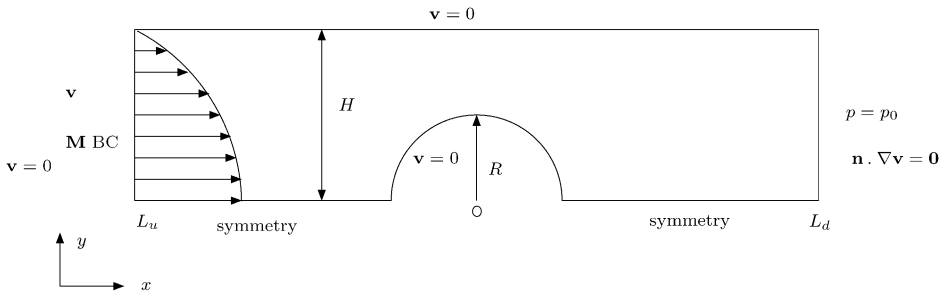

Fig. 6. Geometry and boundary conditions for the two-dimensional flow around a cylinder. **M** BC denotes that different conformation boundary conditions were imposed there.

$$L_{yx} = \left[-\Delta p \frac{b}{L}\left(\frac{y}{b} - \frac{1}{2}\right) + 1\right]\frac{u_0}{b} \tag{17}$$

$$M_{yy} = 1 \tag{18}$$

$$M_{xy} = \lambda L_{yx} \tag{19}$$

$$M_{xx} = 1 + 2\lambda^2 L_{yx}^2 \tag{20}$$

and the remaining components of **L** vanish.

The flow of the Oldroyd-B liquid is computed on a 16 × 16 mesh (Fig. 2); the computed velocity vectors and contours of conformation components M_{xy} and M_{xx} are also shown in Fig. 2. As expected, both inflow and outflow sections are present at the two ends of the flow domain and the contours of M_{xy} and M_{xx} are straight lines parallel to the channel walls. Fig. 3 compares the streamwise normal conformation component M_{xx} computed at $We = 5$ at the right ($x = L$) boundary of the flow with the analytical expression $M_{xx} = 1 + 2(\lambda L_{yx}(y))^2 \equiv 1 + 2We(y)^2$; the agreement is excellent.

The numerical results are compared with the analytical solution point by point. Table 2 shows the error of velocity and conformation tensor at $We = 1, 3.77, 5$, and 9.28 when the new conformation boundary condition is imposed on the inflow regions. Of course, the error grows with We because linear basis functions are used to approximate the components of **M**, whereas the streamwise component of **M** depends quadratically on the cross-stream coordinate. For comparison, Table 3 shows the error on the computed velocity and conformation components at $We = 3$ and 3.77 when no conformation boundary condition is imposed at all. Interestingly, when the Weissenberg number is low (below 3 in this case), not imposing a boundary condition yields little error; however, as soon as the Weissenberg number grows beyond a critical value, omitting the boundary condition yields large errors. In this case, at $We = 3.77$ the relative error on the streamwise conformation component is nearly 50% if no boundary condition is imposed, whereas it is below 0.7% if the boundary condition is imposed.

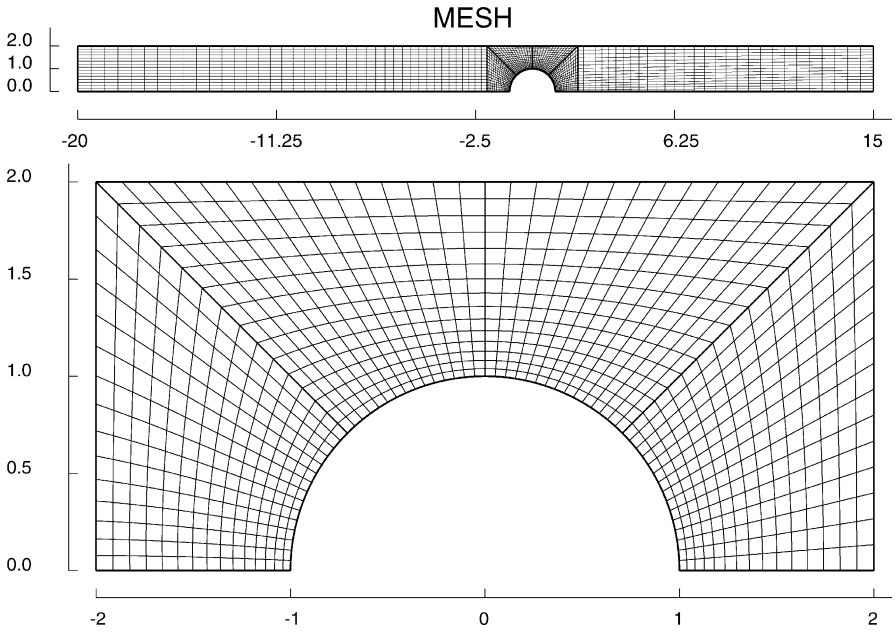

Fig. 7. Mesh of the two-dimensional flow around a cylinder. Top: the whole domain mesh with $L_u = 20R$; bottom: magnified mesh of the region $-2R \le x \le 2R$.

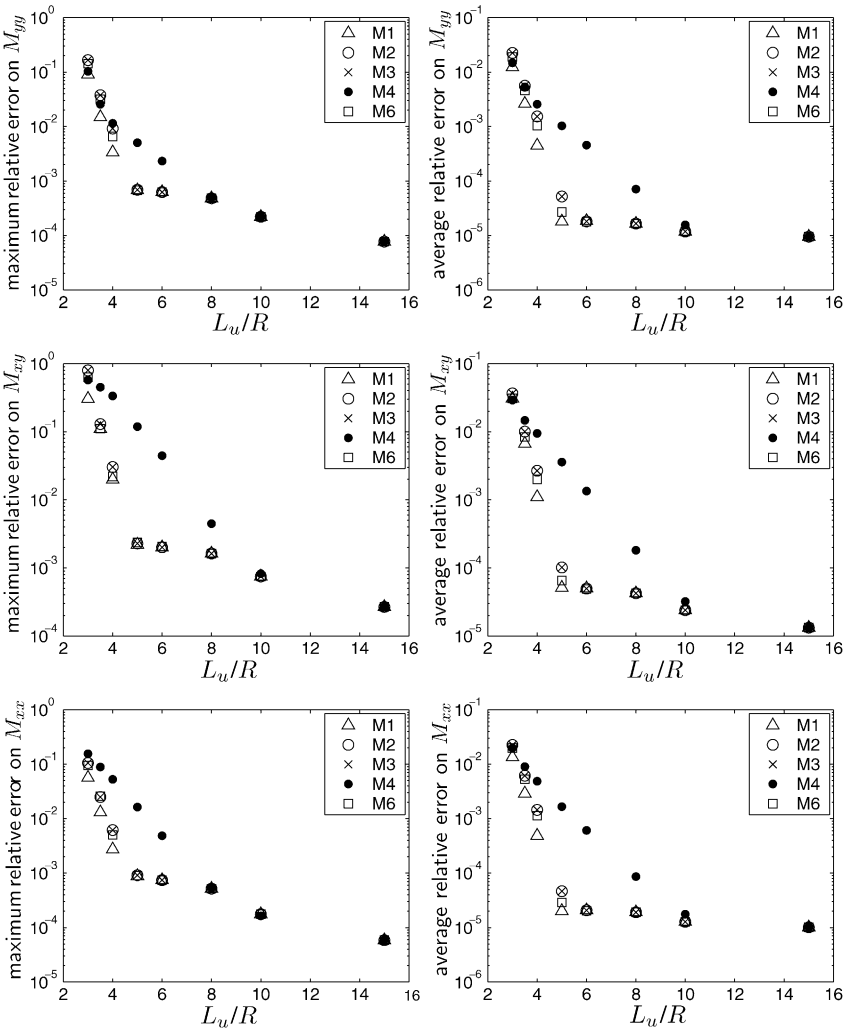

Fig. 8. Comparison of the errors on the conformation components obtained with different conformation inflow boundary conditions in a two-dimensional flow around a cylinder at $We = 0.6$. Left: maximum relative error $e_{M_{ij}}$ (Eq. (31)); right: average relative error $\bar{e}_{M_{ij}}$ (Eq. (32)).

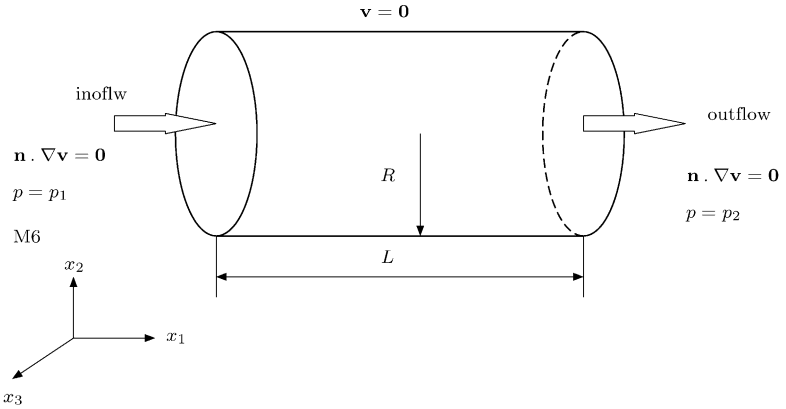

Fig. 9. Geometry and boundary conditions for the three-dimensional flow in a cylindrical pipe.

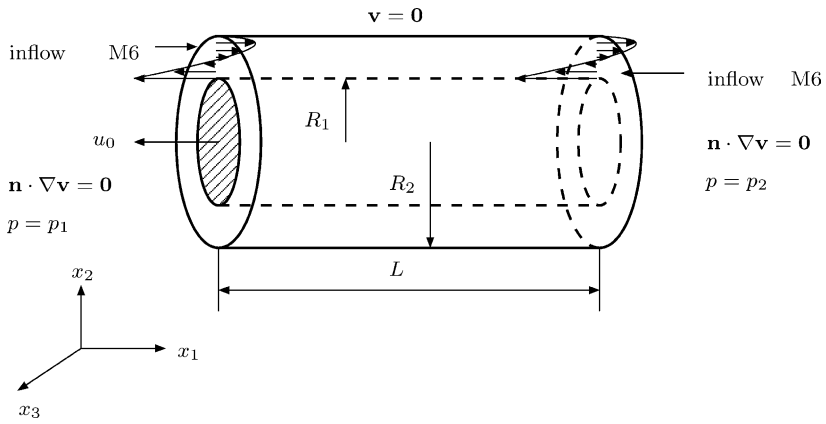

Fig. 10. Geometry and boundary conditions for the three-dimensional flow in a cylindrical annulus. The pressure difference drives flow from left to right, the moving inner cylinder drags flow from right to left; thus, both open-flow boundaries have inflow and outflow sections.

Table 4 shows the computational error on conformation at $We = 3$ on different meshes with the Oldroyd-B fluid. The maximum relative error of M_{11} versus element size is plotted in log-log in Fig. 4 and shows that with mesh refinement the finite element solution is converging to the analytical solution. The extrapolated convergence rate is 1.89, which is slightly higher than the theoretical value of 1.5 for methods based on EVSS/SUPG and linear basis functions [49] (the theoretical result is based on linear basis functions on triangular elements; here we use bilinear basis functions on rectangular elements, which are known to yield superconvergence in certain cases [50,51]).

The Giesekus model is also tested in channel flow on a 40×40 mesh; the parameter α is chosen to be 0.1, the ratio of the solvent viscosity to the (zero-shear) total viscosity is kept at $\beta = 0.59$. The analytical expressions of the components of the conformation tensor can be easily obtained in shear flow [8]

$$M_{xy} = \frac{(1-f)^2}{1+(1-2\alpha)f}\lambda L_{yx} \tag{21}$$

$$M_{xx} - M_{yy} = 2\frac{f(1-\alpha f)}{(\lambda L_{yx})^2\alpha(1-f)}\lambda^2 L_{yx}^2 \tag{22}$$

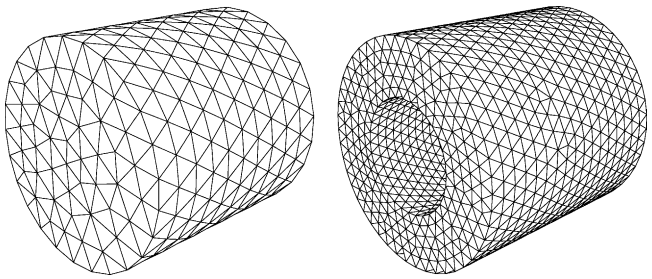

Fig. 11. Unstructured finite element meshes used for computing flow in a cylindrical pipe (left, mesh size $0.25R$) and in a cylindrical annulus (right, mesh size $0.11R_2$ on the inner wall and $0.14R_2$ on the outer wall).

where f and χ are two auxiliary functions

$$f = \frac{1-\chi}{1+(1-2\alpha)\chi} \tag{23}$$

$$\chi^2 = \frac{(1+16\alpha(1-\alpha)(\lambda L_{yx})^2)^{1/2}-1}{8\alpha(1-\alpha)(\lambda L_{yx})^2} \tag{24}$$

Fig. 5 compares the analytical solution to the conformation components M_{xy} (left) and $M_{xx} - M_{yy}$ (right) computed at $We = 11.60$ at the channel sections $x = 0$, $x = L/2$, and $x = L$; the computed results are almost indistinguishable from the analytical solution in all three sections of the flow, showing that the boundary condition works well when applied to a nonlinear conformation model.

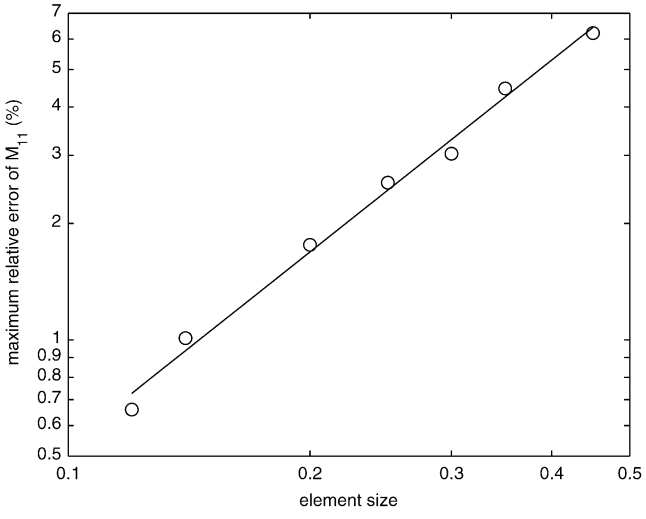

Fig. 12. Convergence rate of the solution computed in the flow in the cylindrical pipe with the Oldroyd-B model at $\beta = 0.59$, $We = 1$. The symbols denote the maximum relative error e on the conformation component M_{11} vs. the dimensionless element size h. The solid line is the best fit $\log(e) = 1.65\log(h) + 1.38$.

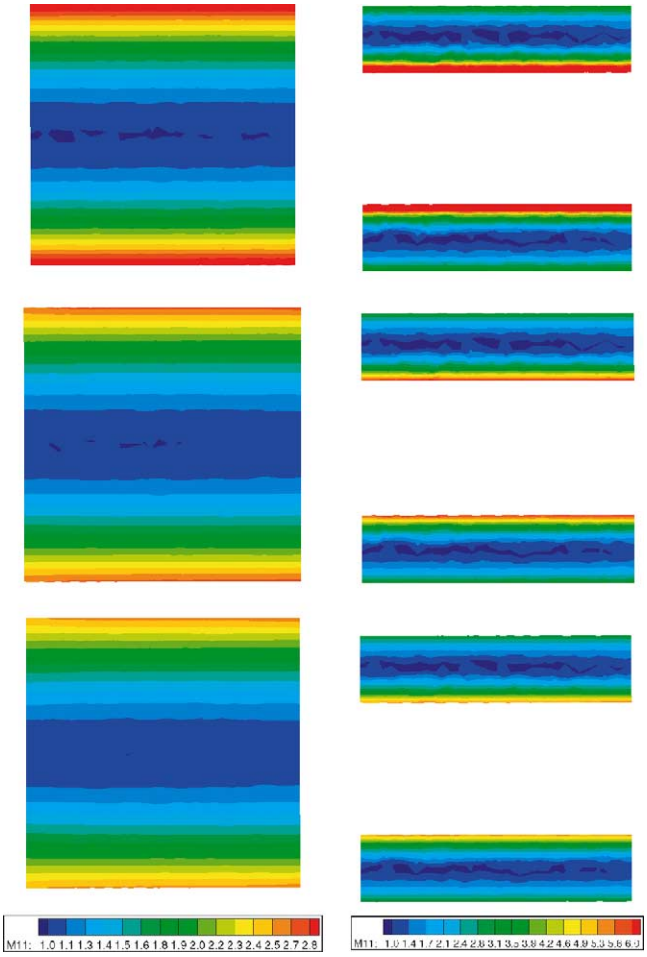

Fig. 13. (color online). Contours of conformation component M_{11} at the $y = 0$ plane computed at $\beta = 0.59$ with the Oldroyd-B (top row), FENE-P ($b = 10$, middle row) and Giesekus ($\alpha = 0.1$, bottom row) models. Left: three-dimensional pipe flow, $We = 1$, characteristic mesh size $0.14R$; right: three-dimensional annular flow, $We = 2$, characteristic mesh size $0.14R$.

5.2. Two-dimensional flow around a cylinder

The new boundary condition is further tested in a two-dimensional flow around a cylinder by varying the upstream length and comparing different boundary conditions. Fig. 6 shows a schematic diagram of the flow and details the boundary conditions. The channel height is $H = 2R$, the downstream length is fixed at $L_d = 15R$, which was found to be sufficient in earlier studies [52]. The upstream section is progressively shortened by decreasing L_u from $L_u = 20R$ to $L_u = 3R$.

The computation is carried out with the Oldroyd-B model at the conditions: flow rate $Q = 1$, $\beta = 0.59$, $We \equiv \lambda(Q/H)/R = 0.6$. At the inflow, the analytical expressions of the velocity and stresses for the Oldroyd-B fluid are

$$v_x = \frac{3Q}{2H}\left(1 - \left(\frac{y}{H}\right)^2\right) \tag{25}$$

$$v_y = 0 \tag{26}$$

$$L_{yx} = -\frac{3Qy}{H^3} \tag{27}$$

$$M_{yy} = 1 \tag{28}$$

$$M_{xy} = \lambda L_{yx} \tag{29}$$

$$M_{xx} = 1 + 2\lambda^2 L_{yx}^2 \tag{30}$$

The flow is first computed at $L_u = 20R$ on the Mesh shown in Fig. 7. For comparison, different methods (M1, M2, M3, M4, and M6) are used to impose boundary conditions at the inflow. Method M5 is not used here because it gives the same results as M1 but is very cumbersome to apply because it requires precomputing the flow in a straight channel. Method M2 is also difficult to implement if periodicity is imposed over a length which exceeds that of one element because it couples elements which are not neighboring each other and thus introduces non-locality in the Jacobian matrix. Therefore, we impose M2 by enforcing periodicity along the flow direction in the first "column" of elements at the inflow boundary.[1]

The computations performed by using methods M2, M3, M4, and M6 differ from the computations obtained with method M1 by less than 10^{-8} in absolute value at any node when $L_u = 20R$; thus the upstream length is sufficiently long and the results obtained with $L_u = 20R$ and method M1 are used as reference solution for comparing with shorter upstream length cases. The reference solution is denoted by the superscript 'o'.

The accuracy of solutions obtained with shorter upstream lengths is assessed by calculating the maximum relative error on each of the computed components of velocity, conformation, velocity gradient, and on the pressure in the region near the cylinder, $-2R < x \leq 2R$.[2] The average relative error is also computed to assess the quality of the solution. For example, the maximum and average relative errors on conformation component M_{ij} are respectively

$$e_{M_{ij}} \equiv \max_k \frac{|M_{ij}(k) - M_{ij}^{o}(k)|}{|M_{ij}^{o}(k)|} \tag{31}$$

$$\bar{e}_{M_{ij}} \equiv \frac{1}{N_{\mathbf{M}}} \sum_{k=1}^{N_{\mathbf{M}}} \frac{|M_{ij}(k) - M_{ij}^{o}(k)|}{|M_{ij}^{o}(k)|} \tag{32}$$

where k is the node counter and $N_{\mathbf{M}}$ is the number of conformation mesh nodes in the region $-2R < x \leq 2R$. Fig. 8 reports the maximum (left) and average (right) error on the conformation components. The errors on the other variables are comparable or smaller, and the off-diagonal component of the conformation tensor M_{xy} dominates the error as the

[1] Because periodicity is imposed over the first column of element instead of over a prescribed length, the upstream length required for obtaining satisfactory results with method M2 is *underestimated* here.

[2] If the absolute value of the variable in the reference solution is below 0.04, then the absolute error is used in place of the relative error.

domain is shortened. When $L_u \geq 10R$, all the boundary conditions yield the same error at the same upstream length; M4 yields considerably higher errors than the other methods when $4R \lesssim L_u \lesssim 8R$. If the criterion is used that a solution should differ from the reference solution at any node by at most 1%, then method M4 fails at $L_u \approx 7R$, whereas M1, M2, M3, and M6 all fail when $L_u \approx 4R$. None of the methods produces an acceptable solution when $L_u < 4R$. Plots of the average relative error (Fig. 8, right) show that when $4R \leq L_u \leq 8R$ M1 is marginally better than M6, which is marginally better than M2 and M3; thus, methods M1, M2, M3, and M6 are roughly equivalent in terms of required upstream length. However, M2 and M3 are not applicable to unstructured meshes and M1 is not applicable to general constitutive equations.

5.3. Three-dimensional flow in a pipe and an annulus

The new boundary condition is tested here in two three-dimensional flows using unstructured meshes: flow in a cylindrical pipe with radius R and length $L \equiv 2R$ and flow in a cylindrical annulus with outer radius R_2, inner radius $R_1 \equiv R_2/2$, and length $L \equiv 2R_2$; Figs. 9 and 10 report the geometric dimensions and the boundary conditions. Hereafter, x_1 denotes the axial coordinate and x_2 and x_3 denote coordinates along two mutually perpendicular radial axes.

In both cases, a pressure difference $\Delta P = p_1 - p_2$ is imposed between the two open sections of the flow through the traction term in the weighted residuals of the momentum equation (see Eq. (11)). The outer cylindrical walls have zero velocity in both flows; in the annular flow, the inner cylinder is moving with velocity u_0 in the direction of decreasing axial coordinate x_1. Thus, the annular flow is a combination of pressure-driven flow (from left to right) and drag flow (from right to left), and both open sections of the annular flow include an inflow and an outflow portion.

The Oldroyd-B model is used in both flows because in the Oldroyd-B model the shear viscosity is constant and thus the velocity and shear rate profiles coincide with those of a Newtonian flow in pure shear flows. Both flows are axisymmetric but are computed as fully three-dimensional.

In both cases, the axial velocity is the only non-zero velocity component. The non-trivial components of velocity and velocity gradient in the cylindrical channel flow are

$$v_1 = \frac{\Delta P R^2}{4\mu L}\left[1 - \left(\frac{x_2}{R}\right)^2 - \left(\frac{x_3}{R}\right)^2\right] \tag{33}$$

$$L_{21} = -\frac{\Delta P}{2\mu L} x_2 \tag{34}$$

$$L_{31} = -\frac{\Delta P}{2\mu L} x_3 \tag{35}$$

and in the annular flow are

$$v_1 = \frac{\Delta P R_2^2}{4\mu L}\left(1 - \left(\frac{x_2}{R_2}\right)^2 - \left(\frac{x_3}{R_2}\right)^2\right) + \frac{\Delta P R_2^2}{4\mu L}\frac{1}{\ln(R_2/R_1)} \times \left[\left(1 - \left(\frac{R_1}{R_2}\right)^2\right)\ln\sqrt{\left(\frac{x_2}{R_2}\right)^2 + \left(\frac{x_3}{R_2}\right)^2}\right] + \frac{u_0}{\ln(R_2/R_1)}\left(\ln\sqrt{\left(\frac{x_2}{R_2}\right)^2 + \left(\frac{x_3}{R_2}\right)^2}\right) \tag{36}$$

$$L_{21} = \frac{-\Delta P x_2}{2\mu L} + \left[\frac{\Delta P R_2^2}{4\mu L}\left(1 - \left(\frac{R_1}{R_2}\right)^2\right) + u_0\right] \times \frac{1}{\ln(R_2/R_1)}\frac{x_2}{x_2^2 + x_3^2} \tag{37}$$

$$L_{31} = \frac{-\Delta P x_3}{2\mu L} + \left[\frac{\Delta P R_2^2}{4\mu L}\left(1 - \left(\frac{R_1}{R_2}\right)^2\right) + u_0\right] \times \frac{1}{\ln(R_2/R_1)}\frac{x_3}{x_2^2 + x_3^2} \tag{38}$$

The conformation components have the same expressions in the two flows

$$M_{11} = 1 + 2\lambda^2(L_{21}^2 + L_{31}^2) \tag{39}$$

$$M_{12} = \lambda L_{21} \tag{40}$$

$$M_{13} = \lambda L_{31} \tag{41}$$

$$M_{22} = 1 \tag{42}$$

$$M_{23} = 0 \tag{43}$$

$$M_{33} = 1 \tag{44}$$

The Weissenberg number is based on the Newtonian velocity profile and is $We \equiv 4\lambda Q/(\pi R^3) = \lambda \Delta P R/(2\mu L)$ in pipe flow and $We \equiv \lambda[(-\Delta P R_1)/(2\mu L) + [\Delta P R_2^2/(4\mu L)(1 - (R_1/R_2)^2) + u_0]/(R_1 \ln(R_2/R_1))]$ in annular flow.

The pipe flow is computed on seven different meshes (Table 6); the mesh with average element size $0.25R$ is shown in Fig. 11 (left). Table 5 shows the error on the computed conformation components at $We = 1$, 2, and 4 on the mesh with average size $0.25R$. The agreement is good, although it degrades as the Weissenberg number grows because the linear conformation basis functions cannot capture well the axial normal conformation profile, which is quadratic in the radial direction.

Table 6 shows the computational error on the conformation components on a set of different meshes at $We = 1$, and Fig. 12 displays the maximum relative error on the axial normal conformation component M_{11} versus the characteristic element size h. The logarithmic plot shows that the

error drops as $\approx h^{1.65}$, in accord with theoretical estimates for SUPG with linear basis functions applied to hyperbolic equations [53] as well as results for EVSS/SUPG methods for viscoelastic flow [49] (the basis functions used here in three dimensional flows are linear). Thus, the new boundary condition works correctly in three-dimensional flows with unstructured meshes.

The FENE-P and Giesekus models are also solved in pipe flow. Fig. 13 (left) shows the comparison between the conformation component M_{11} in pipe flow computed with the Oldroyd-B, FENE-P ($b = 10$), and Giesekus ($\alpha = 0.1$) models, computed on a mesh with average size $0.14R$. As expected, the contours are straight lines along x_1-direction (the small jaggedness is introduced by the interpolation routines of the postprocessor). Naturally, the Oldroyd-B model predicts the highest values of streamwise conformation, whereas (for this choice of parameters) the Giesekus model yields the least distorted conformation.

Fig. 11 (right) shows the mesh used for computing the annular flow; the element size is 0.11 to $0.14R_2$ because the volume mesh is generated based on face mesh size $0.11R_2$ on the inner cylindrical face and $0.14R_2$ on the outer cylindrical face. This mesh has 30189 nodes, 19691 elements and 159047 unknowns. The computations are performed at $\beta = 0.59$, $\Delta P^* \equiv \Delta P R_2/(\mu u_0) = 100$, and $We = 0.70$ to 2.

The computed conformation components are compared to the analytical solutions in Table 7. As in pipe flow (and for the same reasons), the relative error grows with Weissenberg number and is highest in the component M_{11}.

Fig. 13 (right) shows the axial conformation tensor component M_{11} in 3-D annular flow computed at $We = 2$, $\beta = 0.59$, with the Oldroyd-B, FENE-P ($b = 10$), and Giesekus ($\alpha = 0.1$) models. The contours of conformation are nearly straight, as expected, and the axial conformation component is largest near the inner wall, where the shear rate is highest. As in pipe flow, the Oldroyd-B model yields higher axial conformation values than the FENE-P and the Giesekus models.

In summary, the tests reported above show that imposing the new boundary condition on the inflow section of open flow boundaries located in regions of fully developed flow yields correct results in both two- and three-dimensional viscoelastic flows, both when structured and when unstructured meshes are used.

6. Conclusions

Viscoelastic fluids are usually described by rate-type equations for the viscoelastic stress or transport equations for the conformation tensor. Because these equations are hyperbolic (convection-generation) and the streamlines are characteristic lines in steady flows, such equations require boundary conditions at inflow boundaries. A new method is introduced here for imposing inflow conditions in regions of fully-developed, rectilinear flow. The method is based on imposing as an essential boundary condition the algebraic part of the transport equations or conformation tensor equation at the inflow boundary. Tests on simple two- and three-dimensional flows with three different conformation-based models show that the method works well, and that this method retains the best features of earlier methods without having their drawbacks in terms of general applicability to novel conformation-based models, accuracy, computational efficiency, and ability of handling complex situations such as unknown flowrate, inflow-outflow boundaries, and unstructured meshes.

Although new methods which can account for distributions of polymer behavior through stochastic or Fokker–Planck are becoming increasingly important, models based on conformation tensor are still the best candidates for modeling complex process flows because they offer a balance of reasonable accuracy, sound physical grounding, molecular insight, and computational efficiency, which is very important in view of three-dimensional flow calculations, particularly when free-surfaces or deformable boundaries are included [54]. Moreover, coarse-graining efforts underway may soon offer more systematic ways of linking detailed molecular models to conformation based models [55]. The boundary condition introduced here provides a very convenient, accurate, and inexpensive method for building universal computational tools for simulating flows with general coarse-grained models, as well as for solving other hyperbolic problems.

Acknoledgements

The authors thank M. Behr, L. Musson, M. Carvalho, K. Zygourakis, D. Sorensen, Z. Castillo, D. Arora, and B. Khomami for useful discussions. This work was supported by the National Science Foundation (CTS-CAREER-0134389 and CTS-ITR-0312764) and by gifts from ExxonMobil and 3M Corporation. Additional support was provided by Texas ATP grant 003604-0011-2001. Computational resources were provided by the supercomputing facility of the Center for Biological and Environmental Nanotechnology supported by the National Science Foundation Nanoscale Science and Engineering Initiative award EEC-0118007 and by the Rice Terascale Cluster funded by NSF under Grant EIA-0216467, Intel, and HP.

References

[1] R. Keunings, A survey of computational rheology, in: D.M. Binding, N.E. Hudson, J. Mewis, J.-M. Piau, C.J.S. Petrie, P. Townsend, M.H. Wagner, K. Walters (Eds.), Proceedings of the XIIIth International Congress on Rheology, vol. 1, Cambridge University Press, Cambridge, UK, 2000, pp. 7–14.

[2] D. Rajagopalan, R.C. Armstrong, R.A. Brown, Finite element methods for calculation of steady, viscoelastic flows using constitutive equations with a Newtonian viscosity, J. Non-Newtonian Fluid Mech. 36 (1990) 159–192.

[3] F.P.T. Baaijens, Mixed finite element methods for viscoelastic flow analysis: a review, J. Non-Newtonian Fluid Mech. 79 (1998) 361–385.

[4] R.I. Tanner, Engineering Rheology, second ed., Oxford University Press, Oxford, 2000.
[5] M.J. Crochet, A.R. Davies, K. Walters, Numerical Simulation of Non-Newtonian Flow, Elsevier, New York, 1984.
[6] J.M. Marchal, M.J. Crochet, A new mixed finite-element for calculating viscoelastic flow, J. Non-Newtonian Fluid Mech. 26 (1987) 77–114.
[7] R.G. Owens, T.N. Phillips, Computational Rheology, first ed., Imperial College Press, London (2002).
[8] R.B. Bird, R.C. Armstrong, O. Hassager, Dynamics of Polymeric Liquids, second ed., vol. 1, Wiley, New York, 1987.
[9] J.G. Oldroyd, On the formulation of rheological equations of state Proc. R. Soc. Lond., A200 (1950) 523–541.
[10] H. Giesekus, A simple constitutive equation for polymer fluids based on the concept of deformation-dependent tensorial mobility, J. Non-Newtonian Fluid Mech. 11 (1982) 69–109.
[11] A.I. Leonov, Nonequilibrium thermodynamics and rheology of viscoelastic polymer media, Rheol. Acta 25 (1976) 85–98.
[12] A.I. Leonov, A.N. Prokunin, Nonlinear Phenomena in Flows of Viscoelastic Polymer Fluids, first ed., Chapman & Hall, London, 1994.
[13] N. Phan-Thien, R.I. Tanner, A new constitutive equation derived from network theory, J. Non-Newtonian Fluid Mech. 2 (1977) 353–365.
[14] N. Phan-Thien, A nonlinear network viscoelastic model, J. Rheol. 22 (1978) 259–283.
[15] M.D. Chilcott, J.M. Rallison, Creeping flow of dilute polymer solutions past cylinders and spheres, J. Non-Newtonian Fluid Mech. 29 (1988) 381–432.
[16] A.N. Beris, B.J. Edwards, Thermodynamics of Flowing Systems with Internal Microstructure, first ed., Oxford University Press, Oxford, 1994.
[17] M. Grmela, P.J. Carreau, Conformation tensor rheological models, J. Non-Newtonian Fluid Mech. 23 (1987) 271–294.
[18] R.J.J. Jongschaap, K.H. de Haas, C.A.J. Damen, A generic matrix representation of configuration tensor rheological models, J. Rheol. 38 (1994) 769–796.
[19] R. Guénette, Z. Abdelmalek, A. Fortin, P. Carreau, M. Grmela, Simulation of viscoelastic flows using a conformation tensor model, J. Non-Newtonian Fluid Mech. 45 (1992) 187–208.
[20] A.N. Beris, R. Sureshkumar, Simulation of time-dependent viscoelastic channel Poiseuille flow at high Reynolds numbers, Chem. Eng. Sci. 51 (1996) 1451–1471.
[21] R. Sureshkumar, A.N. Beris, R.A. Handler, Direct numerical simulation of the turbulent channel flow of a polymer solution, Phys. Fluids 9 (1997) 743–755.
[22] M. Pasquali, L.E. Scriven, Free surface flows of polymer solutions with models based on the conformation tensor, J. Non-Newtonian Fluid Mech 108 (2002) 363–409.
[23] M. Renardy, W.J. Hrusa, J.A. Nohel, Mathematical Problems in Viscoelasticity, Wiley, New York, 1987.
[24] S.-C. Xue, N. Phan-Thien, R. Tanner, Numerical study of secondary flows of viscoelastic fluid in straight pipes by an implicit finite volume method, J. Non-Newtonian Fluid Mech. 59 (1995) 191–213.
[25] A. Baloch, P. Townsend, M.F. Webster, On vortex development in viscoelastic expansion and contraction flows, J. Non-Newtonian Fluid Mech. 65 (1996) 133–149.
[26] S.-C. Xue, N. Phan-Thien, R. Tanner, Three dimensional numerical simulations of viscoelastic flows through planar contractions, J. Non-Newtonian Fluid Mech. 74 (1998) 195–245.
[27] S.J. Park, S.J. Lee, On the use of the open boundary condition method in the numerical simulation of nonisothermal viscoelastic flow, J. Non-Newtonian Fluid Mech. 87 (1999) 197–214.
[28] K.B. Sunwoo, S.J. Park, S.J. Lee, K.H. Ahna, S.J. Lee, Numerical simulation of three-dimensional viscoelastic flow using the open boundary condition method in coextrusion process, J. Non-Newtonian Fluid Mech. 99 (2001) 125–144.
[29] G. Mompean, M. Deville, Unsteady finite volume simulation of Oldroyd-B fluid through a three-dimensional planar contraction, J. Non-Newtonian Fluid Mech. 72 (1997) 253–279.
[30] M.F. Tomé, N. Mangiavacchi, J.A. Cuminato, A. Castelo, S. McKee, A finite difference technique for simulating unsteady viscoelastic free surface flows, J. Non-Newtonian Fluid Mech. 106 (2002) 61–106.
[31] M. Pasquali, Polymer molecules in free surface coating flows, Ph.D. thesis, University of Minnesota, Minneapolis, MN, available from UMI, Ann Arbor, MI, order number 9963019, 2000.
[32] A.G. Lee, E.S.G. Shaqfeh, B. Khomami, A study of viscoelastic free surface flows by the finite element method: Hele–Shaw and slot coating flows, J. Non-Newtonian Fluid Mech. 108 (2002) 327–362.
[33] R. Guénette, M. Fortin, A new finite element method for computing viscoelastic flows, J. Non-Newtonian Fluid Mech. 60 (1995) 27–52.
[34] M.J. Szady, T.R. Salamon, A.W. Liu, R.C. Armstrong, R.A. Brown, A new mixed finite element method for viscoelastic flows governed by differential constitutive equations, J. Non-Newtonian Fluid Mech. 59 (1995) 215–243.
[35] M. Pasquali, L.E. Scriven, Theoretical modeling of microstructured liquids: a simple thermodynamic approach, J. Non-Newtonian Fluid Mech. 120 (2004) 101–135.
[36] K. Feigl, M. Laso, H.C. Öttinger, CONNFFESSIT approach for solving a two-dimensional viscoelastic fluid problem, Macromolecules 28 (1995) 3261–3274.
[37] X. Gallez, P. Halin, G. Lielens, R. Keunings, V. Legat, The adaptive lagrangian particle method for macroscopic and micro-macro computations of time-dependent viscoelastic flows, Comput. Methods Appl. Mech. Eng. 180 (1999) 345–364.
[38] M.A. Hulsen, A.P.G. van Heel, B.H.A.A. van den Brule, Simulation of viscoelastic flow using Brownian configuration fields, J. Non-Newtonian Fluid Mech. 70 (1997) 79–101.
[39] A. Lozinski, C. Chauviere, J.N. Fang, R.G. Owens, Fokker–Planck simulations of fast flows of melts and concentrated polymer solutions in complex geometries, J. Rheol. 47 (2003) 535–561.
[40] M. Grmela, Dependence of the stress tensor on the intramolecular viscosity, J. Rheol. 33 (1989) 207–231.
[41] V.F. de Almeida, Gas–liquid counterflow through constricted passages, Ph.D. thesis, University of Minnesota, Minneapolis, MN, available from UMI, Ann Arbor, MI, order number 9615160, 1995.
[42] M.S. Carvalho, Roll coating flows in rigid and deformable gaps, Ph.D. thesis, University of Minnesota, Minneapolis, MN, available from UMI, Ann Arbor, MI, order number 9621887, 1996.
[43] T.C. Papanastasiou, N. Malamataris, K. Ellwood, A new outflow boundary-condition, Int. J. Numer. Methods Fluids 14 (1992) 587–608.
[44] D.F. Griffiths, The 'no boundary condition' outflow boundary condition, Int. J. Numer. Methods Fluids 24 (1997) 393–411.
[45] M. Renardy, Imposing 'no' boundary condition at outflow: why does it work?, Int. J. Numer. Methods Fluids 24 (1997) 413–417.
[46] I.S. Duff, A.M. Erisman, J.K. Reid, Direct Methods for Sparse Matrices, first ed., Oxford University Press, Oxford, 1989.
[47] Y. Saad, Iterative Methods for Sparse Linear Systems, second ed., SIAM, Philadelphia, PA, 2003.
[48] G.H. Golub, C.F. Van Loan, Matrix Computations, third ed., The Johns Hopkins University Press, Baltimore, MD, (1996).
[49] D. Sandri, Finite element approximation of viscoelastic fluid flow: existence of approximate solutions and error bounds. Continuous approximation of the stress, SIAM J. Numer. Anal. 32 (1994) 362–377.
[50] E.F. D'Azevedo, Are bilinear quadrilaterals better than linear triangles?, SIAM J. Sci. Comp. 22 (2000) 198–217.
[51] D.N. Arnold, D. Boffi, R.S. Falk, Approximation by quadrilateral finite elements, Math. Comput. 71 (2002) 909–922.
[52] J. Sun, M.D. Smith, R.C. Armstrong, R.A. Brown, Finite element method for viscoelastic flows based on the discrete adaptive viscoelastic stress splitting and the Discontinuous Galerkin method: DAVSS-G/DG, J. Non-Newtonian Fluid Mech. 86 (1999) 281–307.

[53] C. Johnson, Numerical Solutions of Partial Differential Equations by the Finite Element Method, first ed., Studentlitteratur, Lund, Sweden, 1987.
[54] X. Xie, M. Pasquali, Computing 3-D free surface viscoelastic flows, in: A.A. Mammoli, C.A. Brebbia (Eds.), Moving Boundaries VII: Computational Modeling of Free and Moving Boundary Problems, WIT Press, Southampton, UK, 2003, pp. 225–234.
[55] B.J. Edwards, A.N. Beris, Nonequilibrium thermodynamics and complex fluids, J. Non-Newtonian Fluid Mech. 120 (2004) 1–2.